PCCP

PAPER

View Article Online
View Journal | View Issue

Cite this: *Phys. Chem. Chem. Phys.*, 2017, **19**, 21691

In- and Ga-based inorganic double perovskites with direct bandgaps for photovoltaic applications†

Jun Dai,[a] Liang Ma,[a] Minggang Ju,[a] Jinsong Huang[b] and Xiao Cheng Zeng*[ab]

Received 22nd May 2017,
Accepted 18th July 2017

DOI: 10.1039/c7cp03448b

rsc.li/pccp

Double perovskites in the form of $A_2B'B''X_6$ (A = Cs, B′ = Ag, B″ = Bi) have been reported as potential alternatives to lead-containing organometal trihalide perovskites. However, all double perovskites synthesized to date exhibit indirect bandgaps >1.95 eV, which are undesirable for photovoltaic and optoelectronic applications. Herein, we report a comprehensive computer-aided screening of In- and Ga-based double perovskites for potential photovoltaic applications. To this end, several preconditions are implemented for the screening of optimal candidates, which include structural stability, electronic bandgaps, and optical absorption. Importantly, four In- and Ga-based double perovskites are identified to possess direct bandgaps within the desirable range of 0.9–1.6 eV for photovoltaic applications. Dominant optical absorption of the four double perovskites is found to be in the UV range. The structural and thermal stability of the four double perovskites are examined using both the empirical Goldschmidt ratio and convex-hull calculations. Only $Cs_2AgInBr_6$ is predicted to be thermodynamically stable.

Introduction

Solar energy is renewable and sustainable, and the estimated potential of solar energy (1575–49 837 exajoules) is several times greater than the current total world energy consumption.[1] Yet only about 1.1% of the energy consumption originated from solar energy in 2015, implying much higher expectation for photovoltaics in future energy consumption. The recent emergence of organometal trihalide perovskite (OTP) solar cells with power conversion efficiencies (PCEs) reaching as high as 22.1% in 2016[2] offers an unprecedented opportunity for wider use of solar energy. However, current perovskite materials suffer from inherent structure instability; that is, they degrade rapidly upon exposure to water, oxygen, light and high temperature. Moreover, lead (Pb) is a toxic element, and the high content of lead in most OTPs reported has raised special concerns of potential harmful effects to the environment and health.

To address the two issues above regarding the current perovskite technology, growing research efforts have been devoted to the exploration of alternative lead-free materials free of inherent structure instability and degradation under external stimuli, while entailing PCEs close to current perovskite solar cells. In the recent past, high-throughput screening (HTS) of materials has significantly aided the rational materials design and discovery process; for example, Emery *et al.* reported an HTS of perovskites for thermochemical water splitting applications,[3] Castelli *et al.* performed an HTS of perovskite oxides for optimal solar light capture.[4] The computational screening of homovalent lead substitution in OTPs was also reported previously.[5] In previous studies, two group-IV elements, Ge^{2+} and Sn^{2+}, were adopted to replace Pb^{2+} in OTPs. It is found, however, that neither Ge^{2+} nor Sn^{2+} is in their stable oxidization state.[6,7] Bismuth (Bi) is also regarded as a promising element to replace Pb. But Bi exhibits a different oxidization state (+3) from Pb (+2), and thus, direct replacement of Pb^{2+} by Bi^{3+} would alter the perovskite structure and result in the form of $A_3Bi_2I_9$. Indeed, $A_3Bi_2I_9$ (A = Cs^+, MA^+ or FA^+) materials have been synthesized.[8,9] However, the bandgaps of these materials are typically larger than 2.0 eV, unsuitable for photovoltaics. To accommodate Bi^{3+} in the perovskite structure, much effort has been devoted to making double perovskites ($A_2B'B''X_6$), in which the unit cell is twice that of the OTP perovskite. As such, the +2 B site cation in the conventional perovskite (ABX_3) can be split into a +1 B′ cation and a +3 B″ cation. Indeed, a number of inorganic and hybrid organic–inorganic Bi-based double perovskite materials have been reported in the literature recently.[10–16] Inorganic $Cs_2AgBiCl_6$ and $Cs_2AgBiBr_6$ double perovskites experimentally synthesized to date exhibit bandgaps larger than 1.95 eV,[10,12,15]

[a] *Department of Chemistry, University of Nebraska-Lincoln, Lincoln, NE 68588, USA. E-mail: xzeng1@unl.edu*
[b] *Department of Mechanical and Materials Engineering, University of Nebraska-Lincoln, Lincoln, NE 68588, USA*

† Electronic supplementary information (ESI) available: Parameters used for HSE06 hybrid functional; and iso-surface plot of the band-decomposed charge density of $Cs_2CuInCl_6$, $Cs_2AgInBr_6$, $Cs_2CuGaCl_6$ and $Cs_2AgGaBr_6$. See DOI: 10.1039/c7cp03448b

while the bandgap of the hybrid MA_2KBiCl_6 double perovskite is even larger (~3.0 eV).[13] The synthesized $MA_2TlBiBr_6$ double perovskite possesses a bandgap comparable to those of lead halide analogues,[14] but Tl is also a toxic element as Pb. Recent theoretical calculations have predicted a few materials with suitable bandgaps for photovoltaics. For example, one predicted lead-free material is obtained by replacing Pb^{2+} with Bi^{3+} or Sn^{4+} and partially substituting halides with chalcogenides.[17] Several inorganic chalcogenide perovskite materials have also been predicted to have bandgap and absorption properties suitable for photovoltaic applications.[18]

In this work, we report a comprehensive exploration of inorganic double perovskites for potential photovoltaic applications.‡ We predict that four In- and Ga-based double perovskites exhibit bandgaps within the optimal range as solar absorbers (0.9–1.6 eV). Convex-hull analysis shows that only $Cs_2AgInBr_6$ is thermodynamically stable. The computed optical absorption curves show strong peaks in the ultraviolet region, while the absorption in the visible region is not as competitive as popular OTPs.

Computational methods

For perovskites, the Goldschmidt tolerance factor[19] has been widely used as a reliable empirical index to examine the formation of perovskite structures.[20–23] The Goldschmidt tolerance factor is defined as $t = (r_A + r_X)/\sqrt{2}(r_B + r_X)$, where r_A, r_B and r_X represent the radii of the A site cation, B site cation, and X site anion, respectively. Generally, perovskite structures tend to form in the $0.8 \leq t \leq 1.0$ range, although near $t = 0.8$ the perovskite structure is distorted with tilted octahedra.[21] In this work, Shannon ionic radii are used.[24] Similar to a previous work on A site alloying,[20] we use the average of the radii of the two B site cations as r_B, namely, $r_B = 1/2r_{B'} + 1/2r_{B''}$.

All geometry optimizations and electronic structure computations are carried out using density functional theory (DFT) methods within the Perdew–Burke–Ernzerhof generalized gradient approximation (PBE-GGA) as implemented in the Vienna *ab initio* simulation package (VASP 5.4).[25,26] Grimme's DFT-D3 correction is adopted to describe the long-range van der Waals interactions.[27] The ion–electron interaction is treated using the projector-augmented-wave (PAW) technique and a kinetic energy cut-off of 500 eV is chosen. For the geometric optimization, a $11 \times 11 \times 11$ Monkhorst–Pack grid[28] is used, and all structures are relaxed until the forces on the atoms are less than 0.01 eV $Å^{-1}$ while the total energy change becomes less than 1.0×10^{-5} eV. Since the PBE functional tends to underestimate the bandgap, a more accurate hybrid HSE06[29] functional is used to compute the electronic properties. Moreover, spin–orbit coupling (SOC) is also included because previous theoretical calculations have shown that the inclusion of SOC is crucial for correct description of the conduction band edges of Bi- and Sb-based double perovskites.[12]

‡ We noticed a closely related work has been recently published on the synthesis of $Cs_2AgInCl_6$ double perovskite with a direct bandgap of 2.1 eV.[39]

Results and discussion

As shown in Fig. 1, a double perovskite structure can be viewed as double the unit cell of conventional ABX_3 perovskites, and it has the same 12 coordinated A sites and 6 coordinated B sites. However, different from the ABO_3 perovskite, the double perovskite has two cations at B sites (B′ and B″), which may have different orderings. Similar to previous theoretical work,[12] we focus on double perovskites with the rock-salt structure (with space group $Fm\bar{3}m$), in which the cations at B′ and B″ sites are alternatively arranged, with oxidization states of +1 and +3, respectively. The A sites in the double perovskite structure are occupied with Cs^+, the +1 B′ sites are initialized with Cu^+, Ag^+ or Au^+, and halide anions (Cl^-, Br^- or I^-) for the X sites. Instead of the Bi^{3+} and Sb^{3+} reported previously,[12] we select In^{3+} and Ga^{3+} for the B″ sites, both having a stable oxidization state of +3.

The calculated Goldschmidt tolerance factors are summarized in Fig. 2, where the ones for the synthesized $Cs_2AgBiCl_6$ and $Cs_2AgBiBr_6$ are also plotted for comparison. Although a perovskite with t in the 0.9–1.0 range tends to have a perfect structure,[19,20] we adopt the lower limit of $t = 0.84$ at this stage, which corresponds to that of the synthesized $Cs_2AgBiBr_6$ which has a perfect double perovskite structure. As shown in Fig. 2, throughout the compositions considered, 17 out of 18 (except Cs_2AuInI_6) has a tolerance factor $t > 0.84$. Hereafter, we will focus on the properties of these 17 structures with perfect double perovskite structures.

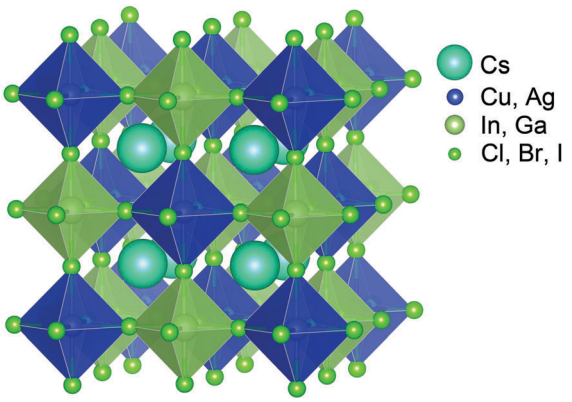

Fig. 1 Crystal structure of rock-salt ordered double perovskite $A_2B'BX_6$ (A = Cs; B′ = Cu, Ag; B = In, Ga; X = Cl, Br, I).

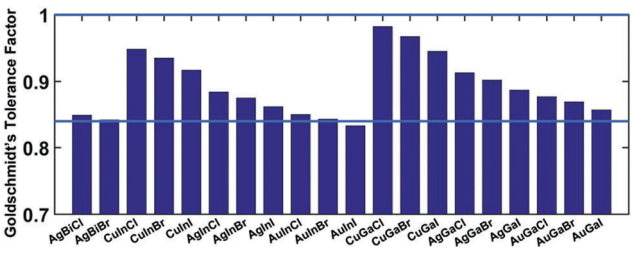

Fig. 2 The calculated Goldschmidt tolerance factors for the double perovskites. For simplicity, we use the B site cations and X site anion to represent a material. For example, AgBiCl represents $Cs_2AgBiCl_6$. The range for perfect double perovskite structures includes those above the horizontal blue line.

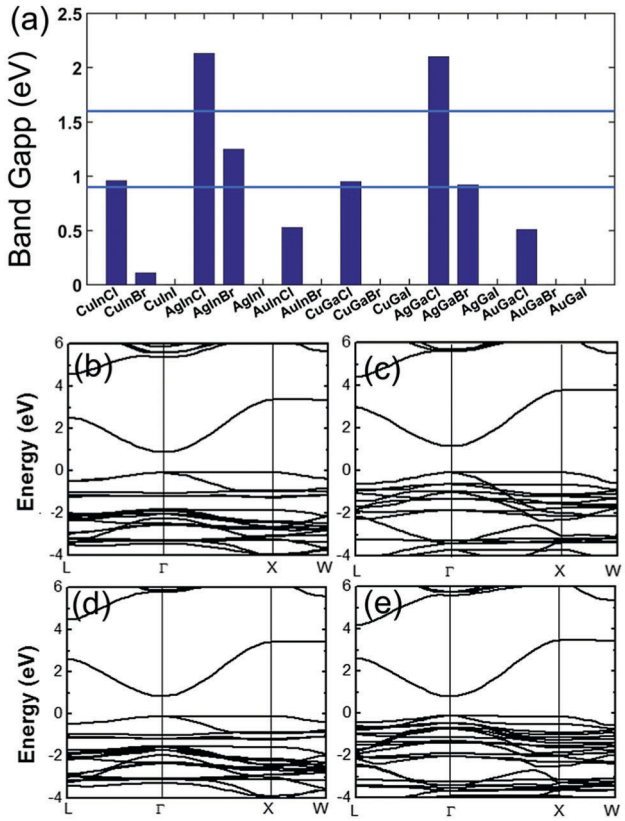

Fig. 3 (a) Computed bandgaps for the double perovskite materials. The range of suitable bandgaps (0.9–1.6 eV) for good absorbers is highlighted between two horizontal blue lines. The ones without vertical bars highlighted are metals. (b–e) Computed HSE06+SOC band structures of (b) $Cs_2CuInCl_6$, (c) $Cs_2AgInBr_6$, (d) $Cs_2CuGaCl_6$ and (e) $Cs_2AgGaBr_6$. Γ (0.0, 0.0, 0.0), X (0.5, 0.0, 0.5), W (0.5, 0.25. 0.75) and L (0.5, 0.5, 0.5) refer to the high-symmetry special points in the first Brillouin zone.

In general, the bandgap of a good absorber material should be within 0.9–1.6 eV, corresponding to a Shockley–Queisser efficiency of $>25\%$.[30] We compute the electronic properties of the 17 double perovskites to see if they meet this precondition. The computed bandgaps for the 17 double perovskites are summarized in Fig. 3. We can see that among the 17 materials, 10 are semiconductors. The bandgaps of the 10 materials lie in a wide range, with the lowest bandgap of 0.11 eV for $Cs_2CuInBr_6$ and the highest bandgap of 2.13 eV for $Cs_2AgInCl_6$. For the double perovskites with the same elements at A, B′ and B″ sites but different halogens, the bandgap decreases from Cl to I, due to the decrease of the ionicity of the elements. Interestingly, we find that among the 10 semiconductors, four have a bandgap within the 0.9–1.6 eV range, namely, $Cs_2CuInCl_6$ (0.96 eV), $Cs_2AgInBr_6$ (1.25 eV), $Cs_2CuGaCl_6$ (0.95 eV) and $Cs_2AgGaBr_6$ (0.92 eV), suggesting that they are good candidates as absorber materials. To gain a better understanding of the electronic properties of $Cs_2CuInCl_6$, $Cs_2AgInBr_6$, $Cs_2CuGaCl_6$ and $Cs_2AgGaBr_6$, we plot their band structures in Fig. 3(b)–(e).

For the four predicted semiconductors with suitable bandgaps, all of them exhibit a direct bandgap, with both the conduction band minimum (CBM) and valence band maximum (VBM) located at Γ. The dispersion of the conduction and valence bands in the vicinity of the Fermi level is quite similar, and compared to the top valence band, and the bandwidth of the bottom conduction band is much larger, indicating better dispersion behaviour. This property can be attributed to the similarity in the band composition, as shown in Fig. S1 (ESI†). The bottom conduction band is mainly contributed by the s states of Cs, while the p and d states of the cations at B sites are accounted for the top valence band. Since the localization decreases from s states to p and d states, a bandwidth narrowing occurs consequently. Another prominent feature is that in all four semiconductors, the two valence bands converge at the valence band maximum, one is flatter than the other. These materials have a relatively small effective mass for electrons ($\sim 0.3m_0$), smaller than the state-of-art $MAPbI_3$ ($\sim 0.4m_e$[31]). On the other hand, for holes, the heavy hole has an effective mass in the 1.6–2.0m_e range, while the light hole is about 0.4m_e.

A good absorbing layer in mono-junction solar cells should also have an absorption coefficient $>10^4$ cm^{-1} to provide at least 80% of light absorption for a film with a thickness of ~ 1 μm.[32] To see whether the predicted four materials meet this precondition or not, we compute the real ($\varepsilon_1(\omega)$) and imaginary ($\varepsilon_2(\omega)$) parts of the frequency dependent dielectric function ($\varepsilon(\omega)$).[33] The computed absorption coefficient is given by $\alpha(\omega) = \frac{\sqrt{2}E}{\hbar}\left[\sqrt{\varepsilon_1^2(\omega)+\varepsilon_2^2(\omega)} - \varepsilon_1(\omega)\right]^{1/2}$, in which E represents phonon energy, and $\hbar$ represents the reduced Planck constant. The computed absorption spectra of the four double perovskites are plotted in Fig. 4. One can see that although all four materials exhibit absorption $>10^4$ cm^{-1} in the 380–450 nm wavelength range (much better than $CsPbI_3$), the overall absorption in the visible-light range is much lower than that of $MAPbI_3$, whose absorption coefficient is of the order of 10^5 cm^{-1}.[34–36] This is because in $MAPbI_3$ the absorption is benefited from p–p transitions,[35,37] while for the systems considered here, the VBM–CBM transitions are predominantly p–s and d–s. Similar results

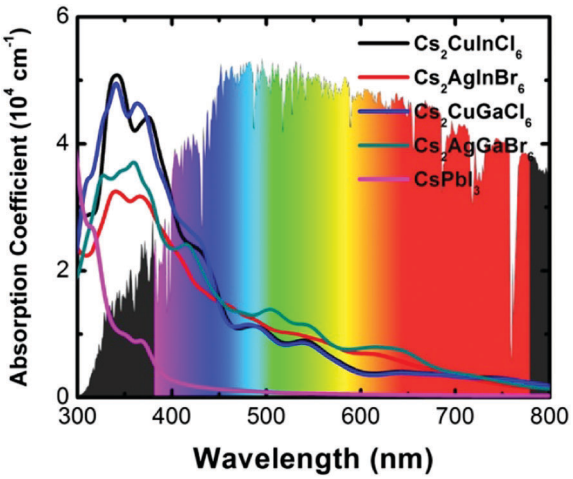

Fig. 4 Computed optical absorption coefficients for the predicted double perovskite materials. The background represents the AM1.5 solar spectrum based on the data from NREL.

have also been discussed by Savory *et al.* recently.[16] Although the delocalized s states in the conduction band are good, the localized d states in the valence band lower the overall absorption efficiency. Note also that a strong peak is present in the ultraviolet (UV) region for all four materials, implying that these materials may be suitable as UV sensors or detectors. Additional treatment of the materials is needed to boost their absorption in the visible range to compete with lead-containing OPTs for applications.

Note that the Goldschmidt tolerance factor is an empirical factor for analysing structural stability. One way to examine the thermal stability of the predicted double perovskites is to check whether they would decompose into other components or not. For an $A_2B'BX_6$ double perovskite material to be stable during its growth, according to the thermodynamic equilibrium condition, the following criteria should be satisfied:

$$2\Delta\mu_A + \Delta\mu_B + \Delta\mu_{B'} + 6\Delta\mu_X = \Delta H_f(A_2BB'X_6), \quad \Delta\mu_i \leq 0\ (i = A, B, B', X),$$

$$a\Delta\mu_A + b\Delta\mu_B + c\Delta\mu_{B'} + d\Delta\mu_X \leq \Delta H_f(A_aB_bB_c'X_d)$$

$\Delta\mu_i = \mu_i - \mu_i^0$ is the deviation of the chemical potential of atomic species i during growth (μ_i) from that of its most stable phase (μ_i^0). ΔH_f is the heat of formation, and $A_aB_bB_c'X_d$ represents all of the existing competing phases. Solutions to these equations give the ranges of $\Delta\mu_i$ being bounded in a polyhedron in a 3-dimensional (3D) space; here we use the 2-dimensional slices of the 3D region by selecting constant $\Delta\mu_i$ for one of the three variables. Our results show that among the four double perovskites only $Cs_2AgInBr_6$ is thermodynamically stable, evidenced by visible dark green polygons as shown in Fig. 5(a) and (b), corresponding to Ag-rich conditions, while the remaining double perovskites predicted show no stable regions, as shown in Fig. 5(c) and (d) for $Cs_2AgGaBr_6$, similar to a closely related report published recently by Zhao *et al.*[38]

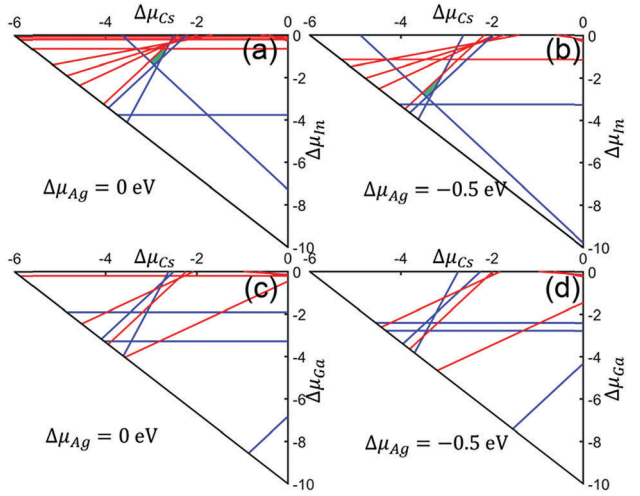

Fig. 5 Computed phase stability diagram analysis results sliced at different Ag-varied growth conditions represented by $\Delta\mu_{Ag}$ (the deviation of the actual chemical potential of Ag from its metal phase) for $Cs_2AgInBr_6$ (a) and (b), and $Cs_2AgGaBr_6$ (c) and (d). The dark green polygon regions in (a) and (b) represent the thermodynamically stable conditions.

Conclusions

In conclusion, we performed a computational screening of In- and Ga-based double perovskites for photovoltaic applications. Four double perovskites exhibit suitable direct bandgaps within the optimal 0.9–1.6 eV range, superior to previously reported Ag/Bi-based double perovskites; however, only $Cs_2AgInBr_6$ is thermodynamically stable. The optical absorption of the double perovskites is predominantly in the UV range.

Acknowledgements

XCZ and JSH were supported by the National Science Foundation (NSF) through the Nebraska Materials Research Science and Engineering Center (MRSEC) (grant no. DMR-1420645), an NSF EPSCoR Track 2 grant (OIA-1538893), and a grant from the Nebraska Center for Energy Sciences Research. Computations were performed using the University of Nebraska Holland Computing Facility.

Notes and references

1 https://en.wikipedia.org/wiki/Solar_energy.
2 NREL record solar cell efficiency table, http://www.nrel.gov/ncpv/images/efficiency_chart.jpg.
3 A. A. Emery, J. E. Saal, S. Kirklin, V. I. Hegde and C. Wolverton, *Chem. Mater.*, 2016, **28**, 5621–5634.
4 I. E. Castelli, T. Olsen, S. Datta, D. D. Landis, S. Dahl, K. S. Thygesen and K. W. Jacobsen, *Energy Environ. Sci.*, 2012, **5**, 5814–5819.
5 (*a*) M. R. Filip and F. Giustino, *J. Phys. Chem. C*, 2015, **120**, 166–173; (*b*) M. G. Ju, J. Dai, L. Ma and X. C. Zeng, *J. Am. Chem. Soc.*, 2017, **139**, 8038–8043; (*c*) L. Ma, J. Dai and X. C. Zeng, *Adv. Energy Mater.*, 2017, **7**, 1601731.
6 C. C. Stoumpos, L. Frazer, D. J. Clark, Y. S. Kim, S. H. Rhim, A. J. Freeman, J. B. Ketterson, J. I. Jang and M. G. Kanatzidis, *J. Am. Chem. Soc.*, 2015, **137**, 6804–6819.
7 N. K. Noel, S. D. Stranks, A. Abate, C. Wehrenfennig, S. Guarnera, A.-A. Haghighirad, A. Sadhanala, G. E. Eperon, S. K. Pathak and M. B. Johnston, *Energy Environ. Sci.*, 2014, **7**, 3061–3068.
8 A. J. Lehner, D. H. Fabini, H. A. Evans, C.-A. Hébert, S. R. Smock, J. Hu, H. Wang, J. W. Zwanziger, M. L. Chabinyc and R. Seshadri, *Chem. Mater.*, 2015, **27**, 7137–7148.
9 B. W. Park, B. Philippe, X. Zhang, H. Rensmo, G. Boschloo and E. M. Johansson, *Adv. Mater.*, 2015, **27**, 6806–6813.
10 A. H. Slavney, T. Hu, A. M. Lindenberg and H. I. Karunadasa, *J. Am. Chem. Soc.*, 2016, **138**, 2138–2141.
11 M. R. Filip, S. Hillman, A. A. Haghighirad, H. J. Snaith and F. Giustino, *J. Phys. Chem. Lett.*, 2016, **7**, 2579–2585.
12 G. Volonakis, M. R. Filip, A. A. Haghighirad, N. Sakai, B. Wenger, H. J. Snaith and F. Giustino, *J. Phys. Chem. Lett.*, 2016, **7**, 1254–1259.
13 F. Wei, Z. Deng, S. Sun, F. Xie, G. Kieslich, D. M. Evans, M. A. Carpenter, P. D. Bristowe and A. K. Cheetham, *Mater. Horiz.*, 2016, **3**, 328–332.

14 Z. Deng, F. Wei, S. Sun, G. Kieslich, A. K. Cheetham and P. D. Bristowe, *J. Mater. Chem. A*, 2016, **4**, 12025–12029.
15 E. T. McClure, M. R. Ball, W. Windl and P. M. Woodward, *Chem. Mater.*, 2016, **28**, 1348–1354.
16 C. N. Savory, A. Walsh and D. O. Scanlon, *ACS Energy Lett.*, 2016, **1**, 949–955.
17 Y.-Y. Sun, J. Shi, J. Lian, W. Gao, M. L. Agiorgousis, P. Zhang and S. Zhang, *Nanoscale*, 2016, **8**, 6284–6289.
18 Y.-Y. Sun, M. L. Agiorgousis, P. Zhang and S. Zhang, *Nano Lett.*, 2015, **15**, 581–585.
19 V. M. Goldschmidt, *Naturwissenschaften*, 1926, **14**, 477–485.
20 Z. Li, M. Yang, J.-S. Park, S.-H. Wei, J. J. Berry and K. Zhu, *Chem. Mater.*, 2015, **28**, 284–292.
21 W. Travis, E. Glover, H. Bronstein, D. Scanlon and R. Palgrave, *Chem. Sci.*, 2016, **7**, 4548–4556.
22 G. Kieslich, S. Sun and A. K. Cheetham, *Chem. Sci.*, 2014, **5**, 4712–4715.
23 G. Kieslich, S. Sun and A. K. Cheetham, *Chem. Sci.*, 2015, **6**, 3430–3433.
24 R. t. Shannon, *Acta Crystallogr., Sect. A: Cryst. Phys., Diffr., Theor. Gen. Crystallogr.*, 1976, **32**, 751–767.
25 G. Kresse and J. Furthmüller, *Phys. Rev. B: Condens. Matter Mater. Phys.*, 1996, **54**, 11169.
26 G. Kresse and J. Furthmüller, *Comput. Mater. Sci.*, 1996, **6**, 15–50.
27 S. Grimme, J. Antony, S. Ehrlich and H. Krieg, *J. Chem. Phys.*, 2010, **132**, 154104.
28 H. J. Monkhorst and J. D. Pack, *Phys. Rev. B: Condens. Matter Mater. Phys.*, 1976, **13**, 5188.
29 J. Heyd, G. E. Scuseria and M. Ernzerhof, *J. Chem. Phys.*, 2006, **124**, 219906.
30 W. Shockley and H. J. Queisser, *J. Appl. Phys.*, 1961, **32**, 510–519.
31 M. R. Filip, C. Verdi and F. Giustino, *J. Phys. Chem. C*, 2015, **119**, 25209–25219.
32 Y. Jin and G. Chumanov, *RSC Adv.*, 2016, **6**, 26392–26397.
33 M. Gajdoš, K. Hummer, G. Kresse, J. Furthmüller and F. Bechstedt, *Phys. Rev. B: Condens. Matter Mater. Phys.*, 2006, **73**, 045112.
34 J. Huang, Y. Shao and Q. Dong, *J. Phys. Chem. Lett.*, 2015, **6**, 3218–3227.
35 W.-J. Yin, T. Shi and Y. Yan, *J. Phys. Chem. C*, 2015, **119**, 5253–5264.
36 C. Zuo, H. J. Bolink, H. Han, J. Huang, D. Cahen and L. Ding, *Adv. Sci.*, 2016, **3**, 1500324.
37 W.-J. Yin, T. Shi and Y. Yan, *Appl. Phys. Lett.*, 2014, **104**, 063903.
38 X.-G. Zhao, D. Yang, Y. Sun, T. Li, L. Zhang, L. Yu and A. Zunger, *J. Am. Chem. Soc.*, 2017, **139**, 6718–6725.
39 G. Volonakis, A. A. Haghighirad, R. L. Milot, W. H. Sio, M. R. Filip, B. Wenger, M. B. Johnston, L. M. Herz, H. J. Snaith and F. Giustino, *J. Phys. Chem. Lett.*, 2017, **8**, 772–778.